RESEARCH ARTICLE

A Novel Strategy for Identifying Non-covalent KRas Inhibitors: Design and Biochemical Characterization of KRas(G12C) Double Mutants for Compound Screening

Authors
Haoshuang Zhao[a], Michael Sabio[a,*], Sid Topiol[a,1], Kuo-Sen Huang[a], Naoko Tanaka[a], Wei Chu[a], Ueli Gubler[a], Peter Tolias[a,b,**]

Affiliations
[a] Center for Healthcare Innovation
[b] Department of Chemistry and Chemical Biology, Stevens Institute of Technology, 507 River Street, Hoboken, New Jersey, USA
[1] Current Address: 3D-2Drug, PO Box 184, Fair Lawn, New Jersey, USA

* Corresponding author.
** Corresponding author.
E-mail addresses: msabio@stevens.edu (M. Sabio), ptolias@stevens.edu (P. Tolias).

Conflicts of Interest: No co-author has any relevant conflicts of interest.

Abstract

By analyzing KRas and HRas X-ray structures, we developed a novel strategy that involves the design of a series of "synthetic" or "artificial" KRas mutations, namely T20I, D57E, D57F, T58A, T58V, and G60A, individually introduced into KRas with the G12C natural pathogenic mutation to create double mutants that we expect would enhance compound binding to the switch II pocket. The goal of using these mutants is to induce greater overall flexibility of the KRas structure to allow the switch II pocket (S-IIP) to open more frequently in the absence of a C12-covalently bound ligand. We developed sensitive assays for the Raf:KRas(GTP) interaction and SOS-driven GDP/GTP exchange to assess these KRas proteins, including the wild-type form, a mutant frequently found in human cancers (G12C), and the "artificial" G12C double mutants. By characterizing these KRas mutants, we hoped to identify at least one mutant that may provide enough flexibility for non-covalent binding to the switch II pocket, thus facilitating future non-covalent compound screening. The results of these assays provide preliminary support that some of the studied mutants demonstrate increased protein flexibility relative to that of KRas(G12C). This strategy of slightly increasing protein flexibility or destabilization through the introduction of selected mutations may be applied to other proteins for which low assay sensitivity is due to transient, high-energy, open-form binding sites.

Keywords: KRas mutations; non-covalent KRas inhibitors; switch II pocket; X-ray crystallography; SOS-driven GDP/GTP exchange; Raf binding activity

1. Introduction

Ras proteins (including the major isoforms of KRas, NRas, and HRas) are small guanine nucleotide-binding proteins that play a crucial role in cell signaling and thus regulation of cell metastasis, proliferation, and survival.[1] They function as molecular switches by cycling between the active GTP-bound state and the inactive GDP-bound state.[2] Ras proteins respond to stimulation with extracellular growth factors, triggering various intracellular signaling cascades.[3,4] In normal cells, the activity of Ras is strictly controlled, with only 4.8% of the available Ras proteins being present in their active conformation.[5] However, in cancer cells, mutant Ras proteins are mainly present in their active conformation.[6,7] The activation process is regulated by guanine nucleotide exchange factors (GEFs), such as the son of sevenless 1, 2 (SOS1, 2) or Ras guanine nucleotide-releasing factor 1 (RasGRF1), which are recruited to the plasma membrane and catalyze the release of GDP from Ras, thus allowing subsequent binding of more prevalent GTP in cells.[8] Upon activation, Ras interacts with signaling effector molecules, thereby triggering the activation of important pathways, such as RAF-MEK-ERK, P13K-AKT-mTOR, and RalGEF-Ral.[9,10]

Ras was identified and characterized as an oncogene over 30 years ago. Its oncogenic mutants play a role in more than 30% of all human cancers.[11] Among all three Ras isoforms, KRas is the most frequently mutated protein in cancer.[12] The most common mutation is at amino acid position 12, which is involved in GAP-mediated GTPase activity. Any mutation at glycine position 12 abolishes GAP-mediated GTPase activity, resulting in a mutant KRas that is continuously activated in cancer cells.[13,14]

The pervasive role of these various oncoproteins in numerous forms of cancer has made them a long sought-after and highly desirable target for small-molecule drug intervention. Nevertheless, these proteins have been rather recalcitrant to traditional and advanced drug-discovery efforts.[15] For many years, the underlying strategy of the discovery efforts for Ras protein inhibitors has been the well-established approach of finding ligands to block the endogenous ligand's active site, i.e., the GDP/GTP site. The lack of success of numerous screening efforts and structure-based studies guided by the availability of extensive protein-structural information can be attributed to the high, picomolar-range affinity of the endogenous GTP and GDP ligands that newly discovered compounds would need to displace. Complicating this approach would be the concurrent need for selectivity against other GDP/GTP targets to prevent undesirable side effects. Analyses of protein structural information had generally concluded that an alternative strategy of targeting an allosteric site was precluded because of a lack of viable alternate binding sites for Ras. In 2012 and 2013, three studies were reported[16–18] for targeting allosteric sites on the oncogenic KRas protein. Two of these sites were in the region of the protein-protein interface between Ras and its activators (e.g., SOS) or downstream signaling partners (e.g., Raf). The third site was targeted for a specific KRas mutant oncoprotein, i.e., G12C, through the pursuit of compounds designed to covalently bind to Cys12 of this mutant protein. Based on this concept, inhibitors, such as ARS-853,[19] that irreversibly bind to KRas(G12C) were developed. ARS-853 binds to KRas(G12C) in an allosteric pocket beneath switch II, which was thus named the switch II pocket (S-IIP).[18] Binding of these inhibitors disturbs both switch I and switch II regions of KRas(G12C), trapping it in its inactive conformation and impairing its binding to downstream effectors such as Raf. The remaining intrinsic GTPase activity of KRas(G12C) can slowly hydrolyze the Ras-bound GTP to GDP,[12] thus effectively turning down KRas signaling.[19,20] The discovery of this novel pocket on KRas renewed the interest in developing direct Ras inhibitors, and stimulated the interest to further study the properties of specific KRas mutants.

In our study, we used structure-based methods to evaluate the three allosteric KRas sites, focusing on the switch II pocket. We describe a new strategy for the eventual discovery of small-molecule, non-covalent inhibitors of KRas. By studying KRas X-ray structures, we designed a series of "synthetic" or "artificial" KRas mutations, namely T20I, D57E, D57F, T58A, T58V, and G60A. Each of these mutants was introduced into KRas already carrying the natural pathogenic G12C mutation. The

prediction is that these mutants will lead to a more flexible KRas structure, allowing the switch II pocket to open more frequently in the absence of a C12-covalently bound compound. Biochemical studies of these mutants are expected to lead to additional insight and understanding of the contribution of this pocket to the overall Ras function. Thus, we developed assays to assess key biochemical characteristics of some of the KRas proteins, including the wild-type form, a mutant frequently found in human cancers (G12C), and the "artificial" G12C double mutants. These assays measured KRas(GTP) binding to Raf and SOS-driven KRas GDP/GTP exchange.

2. Materials and Methods

2.1 Protein Expression and Purification

KRas (UniProtKB-P01116, residues 1-169),[21] NF1-333 (UniProtKB-P21359, residues 1198-1530),[21] cRaf (UniProtKB-Q13114, residues 55-132),[21] and SOS1 (UniProtKB-Q07889, residues 564-1049)[21] coding sequences were synthesized by GenScript.[22] The KRas coding DNA sequence (CDS) was cloned into the pET28b vector with an N-terminal His6 tag, the NF1-333 CDS was cloned into the pGEX-6p-1 vector, the cRaf CDS was cloned into the pGEX-6p-1 vector with an N-terminal Avi tag, and the SOS1 CDS was cloned into the insect cell expression vector pFastBac1 with an N-terminal GST tag. Each construct was engineered to contain a TEV protease cleavage between the tag and the target protein. Expression constructs encoding the KRas mutants were obtained by site-directed mutagenesis of the wild-type construct.

The expression constructs for KRas, NF1-333, and cRaf were transformed into *E. coli* BL21-GOLD (DE3) competent cells (Agilent[23]). *E. coli* cells containing the expression vectors were grown in 2L of Luria broth (LB) with an appropriate antibiotic to an OD600 of 0.6-0.8 and induced with 1mM isopropyl-β-D-thiogalactoside (IPTG) at 23°C overnight. Cells were harvested at 4,000xg for 30min. SOS1 was expressed using the Bac-to-Bac Baculovirus expression system (Invitrogen of ThermoFisher[24]) in *Sf9* cells. Expression conditions using a MOI of 1 and a 48hr culture period were found to be optimal and used in a 6L scale up. Cells were harvest at 4,000xg for 30min.

For the His-tagged KRas protein, cells were harvested, resuspended in lysis buffer (50mM Tris/HCl, pH 7.4, 500mM NaCl, 10mM imidazole, proteinase inhibitor (Roche cOmplete, EDTA-free[25]) at 1g per 10ml), and lysed in a microfluidizer. Debris were pelleted at 34,155xg for 45min, and the supernatant was filtered through a 0.22µm pore size filter. The filtered supernatant was then loaded onto a 25ml Ni-NTA Superflow (Qiagen[26]) column. The column was washed with wash buffer (50mM Tris/HCl, pH 7.4, 500mM NaCl, 10mM imidazole), and the protein was subsequently eluted using a gradient from 0% to 100% elution buffer (50mM Tris/HCl pH 7.4, 500mM NaCl, 500mM imidazole). Fractions containing KRas were identified by SDS-PAGE, and pooled fractions were concentrated using Amicon Ultra-15 centrifugal filter units (10kDa MWCO, MilliporeSigma[25]), followed by further protein purification by size exclusion chromatography using a Superdex 75 16/60 column (GE Healthcare Life Sciences[27]). The purity of the KRas protein in the peak fraction(s) was confirmed by SDS-PAGE, and pooled fractions were again concentrated using Amicon Ultra-15 centrifugal filter units (10kDa MWCO). Protein concentrations were determined by the Bradford Assay (Bio-Rad[28]), using BSA (ThermoFisher[24]) as the standard. After purification, the proteins were exchanged with either GTP or GDP. Approximately 20mg of purified KRas protein in a volume of 6ml were incubated with a 20-fold molar excess of the appropriate nucleotide in 1mM TCEP (Tris (2-carboxyethyl) phosphine hydrochloride) pH 7.4 buffer with 25mM EDTA at 4°C overnight. Subsequently, $MgCl_2$ was added to a final concentration of 30mM, and the samples were incubated for 30min at room temperature. Nucleotide exchanged proteins were filtered through a 0.22µm membrane and then loaded onto a Superdex 75 16/16 column with a running buffer consisting of 50mM HEPES pH 7.5, 200mM NaCl, 10% glycerol, and 1mM TCEP for further purification and to remove excess nucleotides. The purity of peak fractions was established by SDS-PAGE, and appropriate fractions were pooled and concentrated using Amicon Ultra-15 or Ultra-4

(10kDa MWCO). The protein concentration was determined using the Bradford assay. Both GDP- and GTP-exchanged proteins were produced for the following: KRas(WT), KRas(G12C), KRas (G12C/T20I), KRas(G12C/D57E), KRas(G12C/ D57F), KRas(G12C/T58A), KRas(G12C/T58V), and KRas(G12C/G60A). Also, GTP-exchange proteins were produced for KRas(G12V) and KRas(G12D).

cRaf and SOS1 protein purification was performed using GST Sepharose 4B columns (GE Healthcare Life Sciences[27]) followed by size exclusion chromatography using Superdex 200 16/60. Cells were lysed at 1g per 10ml of lysis buffer (25mM HEPES pH 7.4, 300mM NaCl) with proteinase inhibitor as described above by microfluidizer, and pelleted at 34,155xg for 45min. Filtered (0.22µm) supernatant was applied onto a 5ml GST Sepharose 4B column followed by washing with the same buffer. Proteins were eluted with elution buffer (25mM HEPES pH 7.4, 300mM NaCl, 20mM glutathione) and the purity of peak fractions was checked by SDS-PAGE. Appropriate fractions were pooled and concentrated by Amicon Ultrafiltration (30kDa MWCO) and then dialyzed in dialysis buffer (25mM HEPES pH 7.4, 300mM NaCl, 1mM dithiothreitol) at 4°C overnight. Protein concentration was determined by the Bradford assay using BSA as the standard, and protein aliquots were stored at -80°C.

2.2 SOS-driven KRas GDP/GTP Exchange Assay

We developed a KRas(GDP)/GTP exchange assay to study the on-rate of BODIPY labeled GTP (bGTP, Invitrogen of ThermoFisher[24]) binding to KRas(GDP) as triggered by SOS1 (Figure 1). In this assay, we used SOS1 to trigger GDP release. In addition, we used a fluorescence-labeled GTP (bGTP) to measure its exchange rate in different mutant proteins. Typically, His-tagged KRas proteins were pre-loaded with GDP followed by the addition of a Tb-labelled anti-His antibody. SOS1 was then added to trigger the bGTP binding, and TR-FRET signals were measured by Tb-labeled anti-His antibody.

The assay was performed in 50mM Tris/HCl pH7.4, 100mM NaCl, 0.2mg/ml BSA, 0.4mM DTT, and 1mM of $MgCl_2$. A mixture of 140nM KRas(GDP), 4.67nM Tb-coupled anti-His antibody (Invitrogen of ThermoFisher[24]), and 35nM bGTP was prepared and incubated for 30min on ice. The mixture (30µl) was added to a 384-well plate. SOS1 (5µl) protein was added to each well at different dilutions to reach a final concentration of 4µM, 2µM, 1µM, 500nM, 250nM, 125nM, 62.5nM, and 31.25nM. Florescence was measured at 200s intervals over 3200s (Excitation at 320nm; Emission at 495nm and 520nm on the PerkinElmer[29] Envision plate reader). Normalized time-resolved fluorescence resonance energy transfer (TR-FRET) assay signal (Rn) was calculated using the following formulas:

$$Rn = (E_{495}–B_{495}) \bullet [(S_{520}–B_{520}) – C \bullet (S_{495}–B_{495})] / (S_{495}–B_{495})$$

$$C = (E_{520}–B_{520}) / (E_{495}–B_{495})$$

where E_{495} and E_{520} are the fluorescence intensities of 4nM Tb-coupled anti-His antibody at 495nm and 520nm, respectively, B_{495} and B_{520} are the fluorescence intensities of the assay buffer at 495nm and 520nm, respectively, S_{495} and S_{520} are the fluorescence intensities of the samples at 495nm and 520nm, respectively, and C is the cross-talk factor. For each concentration, triplicate data values were obtained, and the average values were then plotted and analyzed with Prism 8 software (GraphPad[30]).

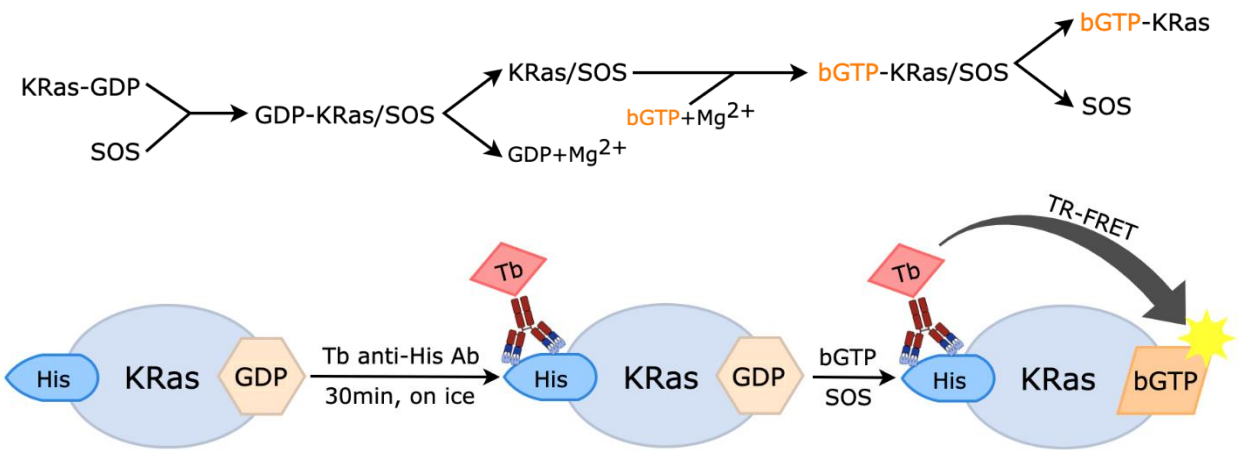

Figure 1. A schematic of the SOS-driven KRas(GDP)/GTP Exchange Assay.

2.3 Testing ARS-853 in the SOS-driven KRas GDP/GTP Exchange Assay

We assayed ARS-853[19] in the SOS-driven KRas GDP/GTP exchange assay, using the same buffer conditions indicated above. 1.2µl of different concentrations of ARS-853 in DMSO starting at 603.33µM (3-fold serial dilution) was incubated with 30µl of 144.8nM KRas(GDP) overnight in a 384-well plate. 5µl of 28.96nM Tb-coupled anti-His antibody, 217.2nM bGTP, and 7.24µM of SOS were added to a 384-well plate. Florescence was measured at 120s intervals over 20min (Excitation at 320nm; Emission at 495nm and 520nm on the PerkinElmer[29] Envision plate reader). Data analysis is identical to the protocol specified in the previous section.

2.4 KRas(GTP)/Raf Interaction Assay

A time-resolved fluorescence resonance energy transfer (TR-FRET) assay was developed to study the affinity of the KRas(GTP)/Raf interaction. KRas(GDP)(320nM) was mixed with 50nM APC-conjugated anti-His antibody (Columbia Biosciences[31]) in 50mM Tris-HCl (pH 7.4), 100mM NaCl, 0.2mg/ml BSA, 0.75mM DTT, and 4mM GTP, and incubated at 23°C for 20min. Raf (250nM) was incubated with Eu-labeled streptavidin (Eu-SA, 0.7nM, PerkinElmer[29]) in 50mM Tris, pH 7.4, 100mM NaCl, 0.75mM DTT, 0.2mg/ml BSA, and 2mM $MgCl_2$ at 23°C for 30min. 15µl KRas/APC-conjugated anti-His antibody solution per well and 15µl of the Raf/Eu-SA solution per well were added onto a 384-plate, followed by 1.4µl of 200mM EDTA. The plate was then centrifuged at 500xg for 1 min, incubated at 23°C for 30min and read on Envision reader (Excitation at 320nm; Emission at 615nm and 665nm). For each KRas protein, triplicate data values were obtained and analyzed with the identical method as described in the previous section.

2.5 Computational Chemistry

We used the Schrödinger software suite[32] to view, superimpose, and compare the collection of Protein Data Bank (PDB)[33] entries for HRas and KRas proteins, some of which are discussed in this report (e.g., PDB:4LYF and PDB:4LV6, each with its covalently bound ligand in the switch II pocket; PDB:2LWI; and PDB:4DSO).

We performed an *in-silico* screening via a high-throughput docking study using the Glide software system[32] and a small database of pharmaceutical molecules, the NIH Pharmaceutical Collection (NPC)[34]. Using the Protein Data Bank (PDB)[33] coordinates of a KRas(G12C) protein (PDB:4LYF), we prepared[35] this study's protein models in the Schrödinger software suite[32]; any of the other PDB entries (e.g., PDB:4LV6) representing KRas(G12C)

with a covalent ligand would have worked as well for this exercise. We deleted all water molecules and the covalent ligand, N-{1-[N-(4,5-dichloro-2-hydroxyphenyl)glycyl]piperidin-4-yl}ethanesulfonamide. We manually adjusted the model, as necessary, to provide appropriate local protein environments by changing the protonation states of selected His, Asp, and Glu residues, the orientation ("flipping") of functionality at the end of specific side chains (i.e., Asn, Gln, and His), and the rotational states of X-H groups (X = O or S). Then all the coordinates were slightly relaxed by using the Protein Preparation module[35] in the Schrödinger software suite.[32]

3. Results and Discussion

3.1 Structure-based Evaluation of Three Reported Allosteric Sites

The three allosteric sites considered herein are shown in Figure 2A. The first site ("A") is near residue Cys12 of the KRas(G12C) mutant.[18] In recent attempts, occupancy of "Site A," which is commonly known as the switch II pocket (S-IIP), is achieved using ligands that covalently bind to Cys12 via a tethering functionality such as a disulfide, acrylamide, or vinyl sulfonamide moiety, as demonstrated with several compounds,[18] such as the ligand in PDB:4LV6. The site is adjacent to the GDP/GTP binding site between the switch I and switch II regions, whose movements are linked to the active (GTP-bound) versus inactive (GDP-bound) states. Compounds bound here were shown to promote the inactive form of these switch regions and correspondingly favor the GDP-bound protein conformation. Note that the switch II pocket (S-IIP) was first identified[36] by an NMR analysis of the interactions of a non-covalent GDP-exchange inhibitor, SCH-54292 (IC_{50} = 700nM), with the HRas-GDP protein. The ligand, whose activity is highly dependent on the metal chelation of its hydroxylamino group, was docked, with guidance from NMR, into a previously unidentified binding cleft in an HRas-GDP crystallographic structure. However, to date, there are no publicly available crystallographic Ras/ligand complexes with compounds in the SCH-54292 series.

The second site ("B") was identified[16] through an NMR screen of small molecules for binding to the KRas(G12D) oncoprotein. The NMR screen identified low-potency compounds (e.g., DCAI with an IC_{50} value of 342μM against nucleotide exchange) that were shown by X-ray structure co-crystallization (e.g., PDB:4DSO, PDB:4DSU, and PDB:4DST) to bind near switch II on the surface of the protein at the region believed to form protein-protein interactions with the guanyl nucleotide exchange factor SOS, a Ras-activating protein. The third site ("C") was identified through examination[37] of the crystal structure (PDB:3KKQ) of the P40D mutant of M-Ras(GTP). This site is close to "Site B" and is believed to represent the Ras/Raf interaction site. *In silico* docking and screening of small molecules at this site identified[17] low-potency Ras/Raf inhibitors (the K_i values in the series are 46μM or greater). In a first step to capitalize on these recent reports for a KRas inhibitor-design program, we examined "Sites A, B, and C" to determine which would be the best to target, or whether, as we ultimately concluded, some alternate strategy or site could be identified.

Both "Sites B and C" are more traditional in that the inhibitors discovered to bind to these sites are non-covalent. Not surprisingly, because they target inhibition of protein-protein interactions, their topologies on the protein surface are shallow. Visual inspection reveals "Site C" to be shallower than "Site B" (Figure 2B). While "Site B" (displayed with benzamidine bound) shows a deeper grove, it is only approximately sized to accommodate a fragment/lead-like compound such as benzamidine (PDB:4DSO), benzimidazole (PDB:4DSU), or 2-(4,6-dichloro-2-methyl-1H-indol-3-yl)ethanamine (PDB:4DST). Thus, both sites appear to be challenging as a starting point for drug design without significantly extending the interaction region. Interestingly, their proximity (Figure 2B) suggests they could be merged into a single target site. "Site A" (the switch II pocket) has characteristics drastically different from those of "Sites B and C." The defining feature of the switch II pocket is the covalent tethering anchor of reactive ligands to Cys12 of the KRas(G12C) mutant. The remainder of each literature ligand reported to bind to the switch II pocket contains hydrophobic/aromatic moieties connected through a linker region to their tethering group. These portions of the inhibitors reside in what appears to be an otherwise attractive (druggable) sub-pocket

(Figure 2C).[18] This sub-pocket under switch II has been described as a hitherto unseen pocket[18] and, excluding the covalent aspect, displays a better druggable character than that of "Sites B and C." This attractive nature of the hydrophobic sub-pocket of "Site A" (compared with "Sites B and C") prompted us to consider whether it could be targeted directly for non-covalent inhibitor design. An anticipated advantage of such an inhibitor would be the elimination of the concern about possible adverse effects of compounds prone to covalent anchoring to cysteine (and/or more general reactivity) as well as the release of the restriction to inhibition of only the KRas(G12C) oncoprotein. This prompted a more careful analysis of the sub-pocket of "Site A."

As mentioned above, visual inspection of "Site A" (the S-IIP) revealed a deep pocket. In addition to the hydrophobic residues, polar residues such as Lys16, Thr58, Arg68, Asp69, His95, and Gln99 are available for defining recognition and selectivity features needed for ligand binding. Generally, tightly binding ligands in such a pocket will show similar, somewhat superimposable structures indicative of a preferred "pharmacophore." Examination of the X-ray structures of several complexes with (covalently bound) ligands revealed, instead, a rather diverse pattern of positions and orientations of even similar ligand functional groups in this sub-pocket.[18] Related to this finding, the range of relative potencies of these inhibitors was only 40-fold.[18] Our interpretation of this observation is that the energetically dominant binding feature of these ligands is still the covalent tethering, with the portions of the ligands residing in the deeper sub-pocket being relegated to less favorable positioning to accommodate the covalent restraint. If this were the case, it would imply that one could find compounds without the covalent tether with more efficient occupancy of this pocket, which ultimately would lead to sufficiently effective binding to achieve suitable potency without a covalent component. In a computational-chemical approach to evaluate this pocket as a viable target, we conducted an *in-silico* screening via a high-throughput docking study using the PDB entry 4LYF, the Glide software system,[32] and a small database of pharmaceutical molecules, the NIH Pharmaceutical Collection (NPC)[34]; any of the other PDB entries (e.g., PDB:4LV6) representing KRas(G12C) with a covalent ligand could also have been used for this exercise. We partitioned the results (data not shown) to display small molecular structures with MW $\leq$ 350 and then a subset with MW $\leq$ 150. In comparison to the results for compounds with MW $\leq$ 350, the smaller molecules show a clear preference for occupying deeper locations within the pocket. These computational probes thereby suggest that this inner region of the pocket is an attractive binding site for which more optimal structures can be sought. For comparison, similar studies were done for "Sites B and C." The results for "Site B" were similar, whereas the results for "Site C" demonstrated that the docked structures drifted away from the site. Overall, we deemed the sub-pocket in "Site A" (the S-IIP) revealed in the relevant X-ray structures to be a suitable target for drug discovery. The next concern was that there did not appear to be evidence of this sub-pocket in the absence (prior to the reporting) of the Cys12 covalently linked inhibitors, as indicated previously.[18] Two possible explanations for the appearance of this sub-pocket with covalently bound inhibitor are (1) the anchoring of the covalent region forces the remainder of the ligand to pry open the protein to expose this sub-pocket and (2) this sub-pocket is a feature of a relatively high-energy protein conformation that has a thermodynamically low frequency of occurrence. A literature-reported "Site A" ligand could thus initially bind to Cys12 covalently, and only when the sub-pocket becomes available, the inhibitor will fill the sub-pocket. We hypothesized that the second explanation is more accurate based on the following arguments. There is considerable flexibility in the region between the α-carbon atom of the Cys12 residue through to the tail-end of each ligand binding in the deepest part of the sub-pocket. This indicates that it is unlikely that the more deeply binding portion of these ligands are forced into the sub-pocket – an event more likely to require a very rigid and direction-limiting linking region. Published X-ray structures provide additional evidence. In fact, one of the KRas X-ray structures of a covalently linked inhibitor (N-{1-[N-(4,5-dichloro-2-ethylphenyl)glycyl]piperidin-4-yl}ethanesulfonamide of PDB:4M1W, Chain A) has the bulk of the ligand directed out of its cavity. In addition, an HRas crystal structure has been reported with the protein in a partially open conformation in the S-IIP region (PDB:4Q21).

This structure, which is partially open supports our hypothesis for opening of this region in the absence of a covalently bound ligand at Cys12. Finally, the initial report of the X-ray structures of the covalently bound ligands also suggested a dynamic nature of the S-IIP.[18]

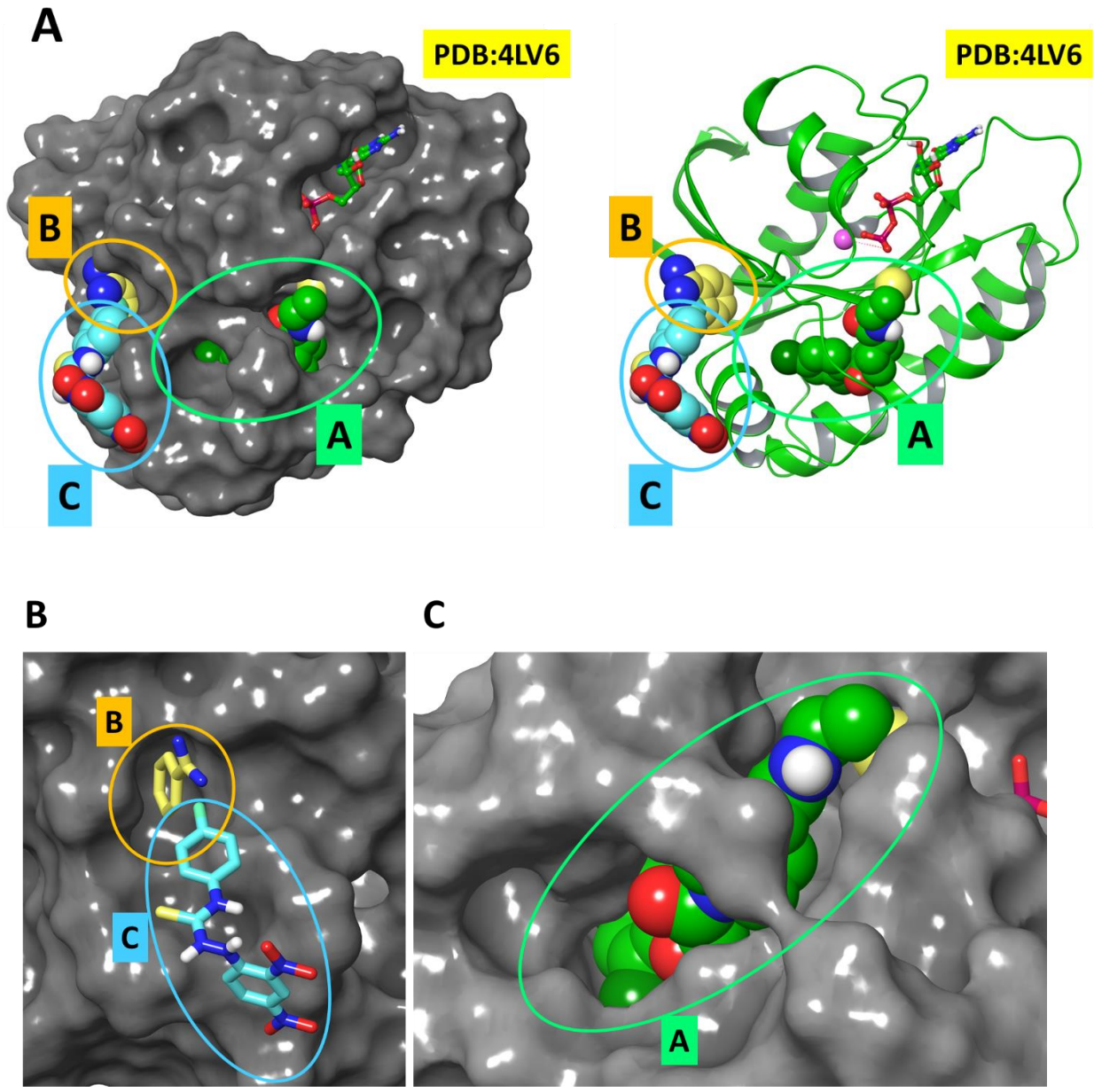

Figure 2. In panel A, KRas "Sites A, B, and C" are indicated on a gray surface rendering of PDB:4LV6 with its covalently bound ligand in "Site A" (the switch II pocket or S-IIP); the ligands from PDB:4DSO (benzamidine) and PDB:2LWI (by NMR: Kobe2601 or 2-(2,4-dinitrophenyl)-N-(4-fluorophenyl) hydrazinecarbothioamide), respectively, are shown at "Sites B and C" after a superimposition of the three KRas X-ray and NMR structures (PDB:4LV6, PDB:4DSO, and PDB:2LWI). Panel B indicates the shallow nature and proximity of "Sites B and C," with the respective ligands of panel A. Panel C indicates the well-defined pocket of "Site A" in the KRas X-ray structure of PDB:4LV6.

3.2 Structure-based Design of Tool Proteins to Screen for S-IIP Inhibitors

Our assumption of the presence of the open form of the S-IIP, when incorporated into a screening paradigm, required a specific strategy to address the statistically low probability (limited availability) of this open form. The failure after decades of focused screening efforts to identify non-covalent binders at this sub-site attests to the likely futility of simply implementing conventional approaches; however, a few non-covalent Ras-binders, including SCH-54292,[36] as described in the previous section, were discovered.[38] Thus, even after using available open-form X-ray structures for *in-silico* screening via high-throughput docking, the testing of selected, top-scoring *in-silico* screening "hits" is unlikely to provide verification or detection of active compounds. We therefore devised a strategy to amplify the sensitivity of our biochemical and biophysical screens through the design of tool proteins with enhanced affinity for binders in the switch II pocket (S-IIP). This strategy of slightly increasing protein flexibility or destabilization through the introduction of selected mutations may be applied to other proteins for which low assay sensitivity is due to transient, high-energy, open-form binding sites.

As observed in Figure 3A, a comparison of an open-form S-IIP KRas(G12C) structure (PDB:4LV6 with 1-[(2,4-dichlorophenoxy)acetyl]-N-(2-sulfanylethyl)piperidine-4-carboxamide covalently bound at S-IIP and GDP in the active site) displayed in gold and a closed-form HRas(G12C) structure (PDB:4L9W with GMPPNP, a GTP analog, in the active site) shown in green reveals the salient structural differences. When compared to the closed form, the open form has the α-helix of switch-II shifted outward and away from the S-IIP, and the attached loop is displaced outward from the pocket, as indicated with red arrows. However, in comparisons of different Ras X-ray structures with and without a covalent ligand bound in the S-IIP, the positions of the α-helix and loop vary, depending on the S-IIP ligand and on the occupant of the GDP/GTP site. In any case, the salient protein conformational differences are most obvious in the switch-II region (as observed for the α-helix and the loop).

An increase of the availability of the "open" KRas form could, therefore, increase the likelihood (i.e., affinity) of ligand-binding. We considered protein residues lining the inner walls of the pocket and postulated that small changes (via mutations) of these residues could slightly destabilize this protein conformation, increasing the presence of the open conformation of the S-IIP, while still maintaining the overall structural and mechanistic integrity of the mutant proteins. Once potential inhibitors are identified by using these tool proteins, albeit possibly inactive in the natural (e.g., oncoprotein) form, they could then be optimized to novel compounds suitably active at natural KRas proteins. Therefore, we could generate potential tool KRas(G12C) proteins, each of which would contain a mutation of one of the residues indicated in Figure 3B: Ser17, Thr20, Ile55, Asp57, Thr58, G60, and Tyr71; in this study, we investigated KRas(G12C) mutated individually with members of a selected subset consisting of T20I, D57E, D57F, T58A, T58V, and G20A.

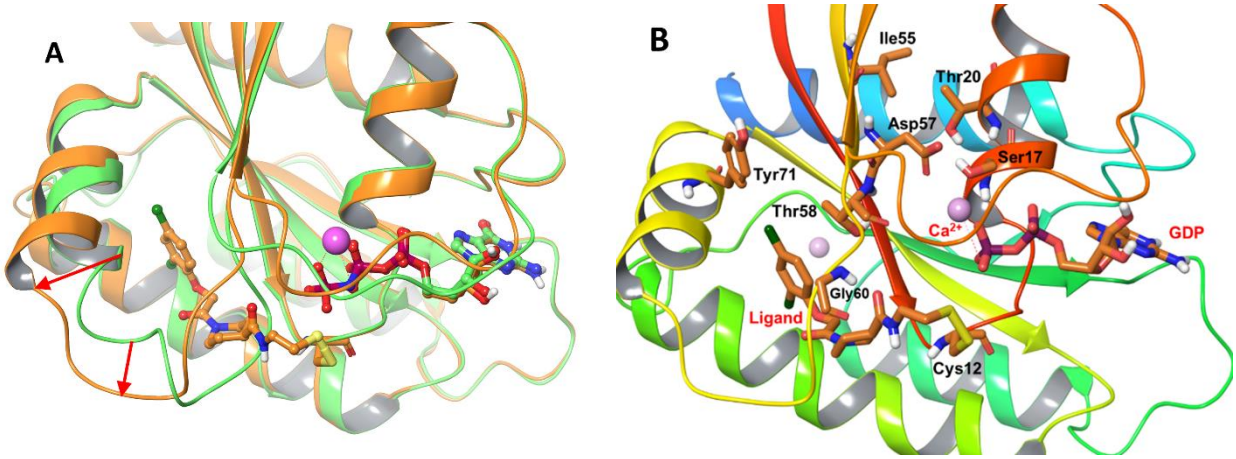

Figure 3. In panel A, salient structural differences are revealed in a comparison (i.e., via a superimposition) of an open-form S-IIP KRas(G12C) structure (PDB:4LV6 with 1-[(2,4-dichlorophenoxy)acetyl]-N-(2-sulfanylethyl)piperidine-4-carboxamide covalently bound in the S-IIP and GDP in the active site) in gold with a closed-form HRas(G12C) structure (PDB:4L9W with GMPPNP, a GTP analog, in the active site) in green. In panel B, the S-IIP of PDB:4LV6 is shown with the labeling of residues that we targeted as part of our novel mutation strategy.

3.3 GDP/GTP Exchange Rates of KRas Mutants

As explained in the previous section, we investigated, in this study, KRas(G12C) mutated individually with T20I, D57E, D57F, T58A, T58V, and G20A. However, we did not know whether these artificial mutants would have properties similar to those of the G12C single mutant and whether the artificial mutants are able to enhance compound binding. To better understand the properties of these double mutants compared to KRas(WT) and the naturally occurring KRas(G12C) single mutant, we developed biochemical assays to study how different KRas mutants affect activation. We developed a TR-FRET assay for measuring GDP/GTP exchange (see Methods). The time-dependent TR-FRET signals at different SOS concentrations for KRas(WT) and KRas(G12C) are shown in the graphs in Figure 4A, and the exchange rates are provided in Figure 4B. Based on these results, the nucleotide exchange rate of KRas(WT) is greater than that of KRas(G12C).

We then determined the GDP/GTP exchange rates of our artificial double mutants. The results are also shown in Figure 4B. The exchange rates of some mutants cannot be determined at lower SOS concentrations, and the maximum exchange rate cannot be reached with 4μM SOS. Therefore, we compared the exchange rates of KRas proteins at 4μM SOS. Among all the double mutants, KRas(G12C/T58V) and KRas(G12C/T58A) showed the highest exchange rates. Their exchange rates are 370% and 311%, respectively, of the KRas(G12C) rate. These exchange rates are 159% and 134%, respectively, of the KRas(WT) rate. In contrast, KRas(G12C/D57E), KRas(G12C/T20I), and KRas(G12C/G60A) showed only 40%, 24%, and 7%, respectively, of the KRas(G12C) rate. Mutations at these three residues significantly reduce GDP/GTP exchange rates. We also determined the exchange rate We suspect that similar IC of the KRas(G12C/D57F) mutant and found that it did not show any significant GDP/GTP exchange activity at any SOS concentration evaluated (data not shown), indicating that this mutant perturbs the protein conformation to an extent that it abolishes GDP/GTP exchange.

A

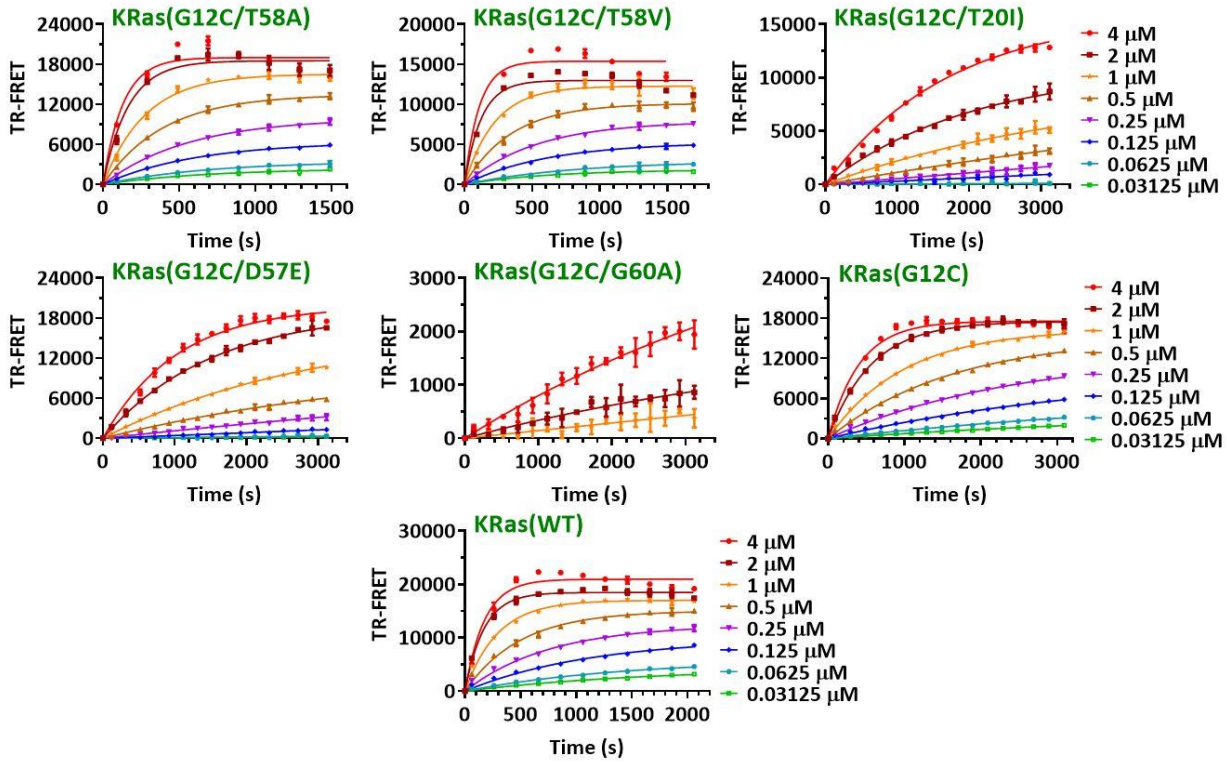

B

KRas(GDP)-GTP Exchange Rate (10^{-4} unit/s)							
SOS conc. (μM)	**4**	**2**	**1**	**0.5**	**0.25**	**0.125**	**0.0625**
KRas(G12C/T58V)	91.1	80.9	45.0	28.6	19.0	16.2	12.2
KRas(G12C/T58A)	76.6	60.1	35.9	25.2	17.8	16.3	14.5
KRas(WT)	57.2	58.5	34.4	20.1	13.2	8.80	6.93
KRas(G12C)	24.6	17.8	10.1	6.13	4.09	2.67	1.76
KRas(G12C/D57E)	9.75	6.65	3.38	2.42	0.683	-	-
KRas(G12C/T20I)	5.79	4.87	2.67	0.991	-	-	-
KRas(G12C/G60A)	1.81	1.79	-	-	-	-	-

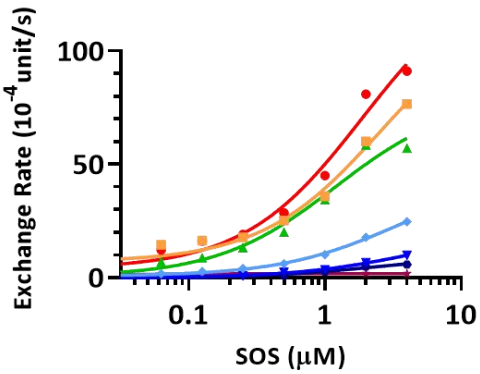

	Exchange rate at 4μM SOS (x10^4)	% cmpr. with KRas(WT)	% cmpr. with KRas(G12C)
KRas(G12C/T58V)	91.1	159	370
KRas(G12C/T58A)	76.6	134	311
KRas(WT)	57.2	100	233
KRas(G12C)	24.6	43	100
KRas(G12C/D57E)	9.75	17	40
KRas(G12C/T20I)	5.79	10	24
KRas(G12C/G60A)	1.81	3	7

Figure 4. (A) The exchange kinetics of KRas(WT), KRas(G12C), and KRas(G12C) double mutants at different SOS concentrations. The data values were plotted by Prism 8 software (GraphPad[30]) using a one-phase association equation: $Y=Y_0+(Plateau-Y_0)*(1-exp(-K*X))$ where Y_0 is the Y value when X (time) is zero; Plateau is the Y value at infinite time; and K is the exchange rate. (B) For KRas(G12C/D57E), KRas(G12C/T20I), and KRas(G12C/G60A)), the exchange rates are too low to be calculated at low SOS concentrations. The KRas(G12C/D57F) mutant did not show any significant GDP/GTP exchange activity at any SOS concentration evaluated (data not shown). The exchange rates were plotted against various SOS concentrations and fit with $Y=Bottom+(Top-Bottom)/(1+10^{((logEC_{50}-X)*Hillslope)})$, where Top and Bottom are plateaus in the units of the Y axis; EC_{50} is the concentration of agonist that gives a response halfway between Bottom and Top; and Hillslope is set to 1.

Molecular modeling of the KRas(G12C) double mutants might explain how the changes interfere with the nucleotide binding site and therefore why the proteins have different exchange rates. The double mutants were designed with the intention that the resulting proteins would become more flexible and that the S-IIP cavity would open more easily and more often. This could be accomplished by the loss of a structurally stabilizing hydrogen bond between residues or the introduction of steric clashes that would separate secondary structural elements, etc., as shown in Figures 5–8.

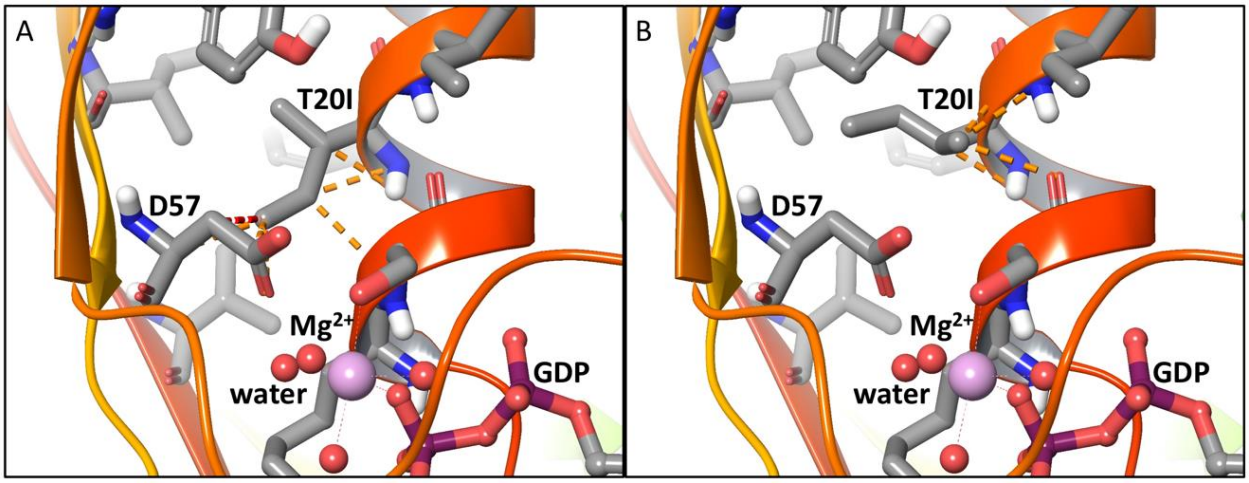

Figure 5. For the KRas(G12C/T20I) model derived from PDB:4LDJ Chain A, two standard side-chain rotational states were selected for residue T20I, as shown in panels A and B. The Ile20 sidechain is bulkier than the naturally occurring Thr side chain and would lead to steric clashes with Asp57 or the helix containing Ile20. To relieve the strain caused by the Ile side chain, a resulting protein conformational change (either by the separation of secondary structural elements or by the disruption of the helix) may displace the nearby metal/water cluster associated with GDP (as shown) or GTP.

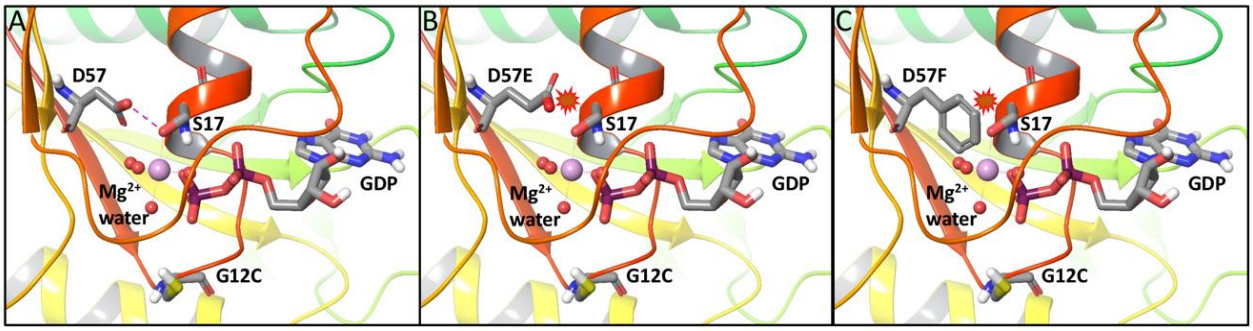

Figure 6. The mutation of Asp57 in KRas(G12C) to either D57E or D57F would lead to a loss of a hydrogen bond, between the carboxyl group of Asp57 and Ser17 (panel A), which is involved in the coordination of the metal ion. Unlike the naturally occurring Asp side chain, the Glu side chain (panel B) is too long to achieve a productive hydrogen bond with Ser17 and might cause a steric clash with Ser17. Similarly, Phe57 (panel C) would not be tolerated in this region of the binding cavity and could displace the metal/water cluster. It appears that the Phe mutation would be more detrimental than the Glu mutation.

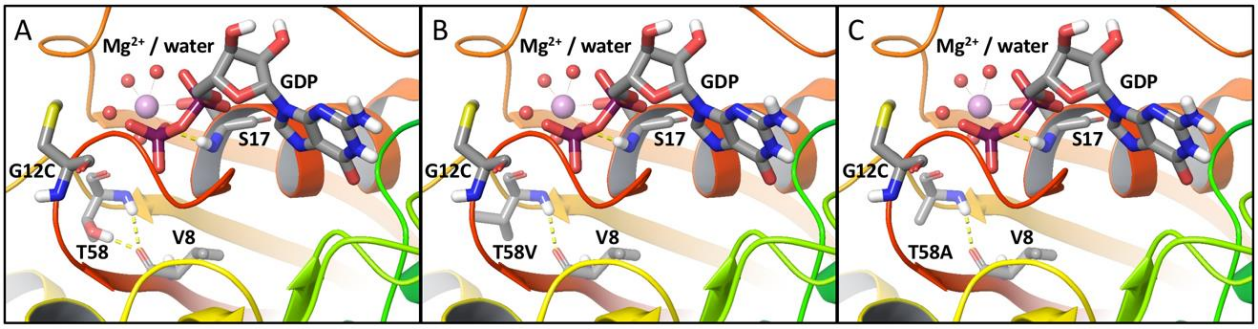

Figure 7. The mutation of Thr58 (panel A) to a Val (panel B) or Ala residue (panel C) was intended as a test of the importance of the Thr58 side-chain hydrogen bond in stabilizing the conformation of the protein. We predicted that the loss of this hydrogen bond would result in greater protein flexibility, especially close to the GDP/GTP binding site.

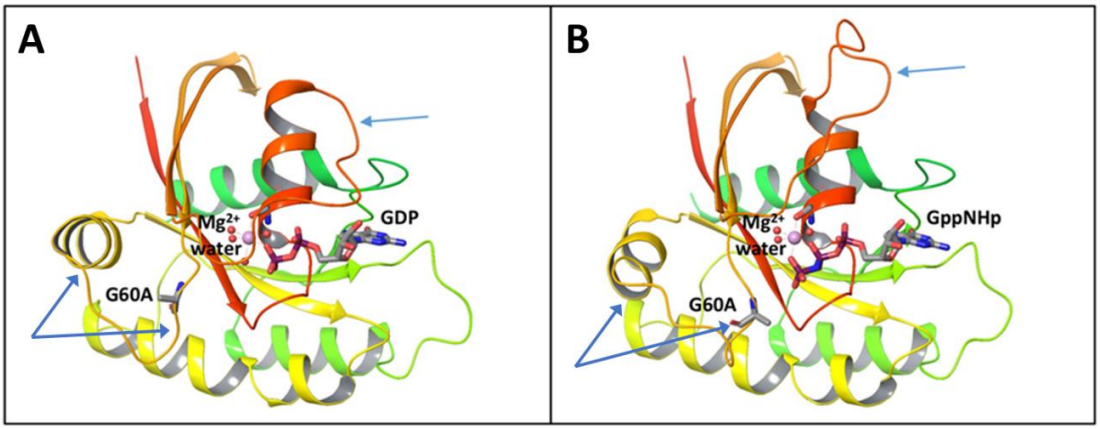

Figure 8. X-ray structures of the homologous HRas(G60A) with GDP (panel A) and a GTP analog (GppNHp) (panel B) were used in this example as surrogates for KRas(G12C/G60A). The significant restructuring (indicated by blue arrows) of the switch I and II regions due to the G60A mutation in the GppNHp-bound structure (panel B) affects the interactions of GppNHp with its binding site.[39]

3.4 The Effect of ARS-853 on SOS-driven KRas GDP/GTP Exchange

Ideally, we would like to determine whether at least one of our designed KRas double mutants has enhanced affinity, relative to that of KRas(G12C), for binders at the S-IIP, due to increased protein flexibility or destabilization, as demonstrated through increased sensitivity in any of our biochemical and biophysical screens. We were curious whether we could detect increased assay sensitivity of some of the artificial double mutants, relative to that of KRas(G12C), to a covalent S-IIP ligand, specifically ARS-853,[19] for which a Ras/ligand X-ray crystallographic complex is publicly available. However, we were also concerned whether the results of assays using various mutants would be largely indicative of the formation of the covalent bond between ARS-853 and Cys12 in the binding of the covalent ligand to the S-IIP, rather than serving as a measure of affinity for the full ligand. If the IC_{50} values in the SOS-driven KRas GDP/GTP exchange assay would be essentially invariant across G12C and the double mutants, we would need to consider that we were measuring the extent of covalent bond formation. The graphs and corresponding IC_{50} values are displayed in Figure 9 for selected KRas mutants. In our biochemical assay, the IC_{50} values for KRas(G12C/T58A), KRas(G12C/T58V), KRas(G12C/T20I), and KRas(G12C/G60A), are sufficiently similar to (i.e., all are within a factor of 4.7 of) the IC_{50} value for KRas(G12C). Moreover, the IC_{50} value of each double mutant is higher than the 180nM value of KRas(G12C). For a comparison to our biochemical assay result, the literature IC_{50} value of 2.5μM[40] pertains to ARS-853's ability to inhibit the proliferation of H358 mutant cells and its ability to inhibit KRas(G12C) in a cell-based assay.

We suspect that the similarity of IC_{50} values of five of the KRas proteins represented in Figure 9 indicates similar ease of covalent-bond formation with Cys12, rather than similar full-ligand binding affinity. In support of this hypothesis, kinetic studies[41,42] explain how KRas(G12C) inhibitors like ARS-853 have a weak binding affinity (e.g., ARS-853's K_i value is 200μM[42]) but demonstrate a very fast chemical reactivity. The authors conclude[41] that Lys16 of KRas(G12C) activates ARS-853's acrylamide electrophile to facilitate the attack by Cys12's nucleophilic sulfur atom and stabilizes the enolate intermediate involved in bond formation. Applying this insight to our study of ARS-853 in our SOS-driven KRas GDP/GTP exchange assay, we surmise that the five similar IC_{50} values are a consequence of a nearly equivalent, unhindered environment around Cys12 for facile bond formation in the five KRas proteins. In contrast, KRas(G12C/D57E) and KRas(G12C/D57F) have considerably higher IC_{50} values, perhaps indicating impeded covalent-bond formation due to significant destabilization or adverse protein conformational changes near Cys12. In essence, due to the facile covalent bond formation in the assays of ARS-853,[19] we did not learn useful information about potential increased assay sensitivity of some of the artificial double mutants, relative to that of KRas(G12C). To eliminate the issue of the contribution of covalent-bond formation to binding affinity, we would need to identify and assay non-covalent binders of the S-IIP.

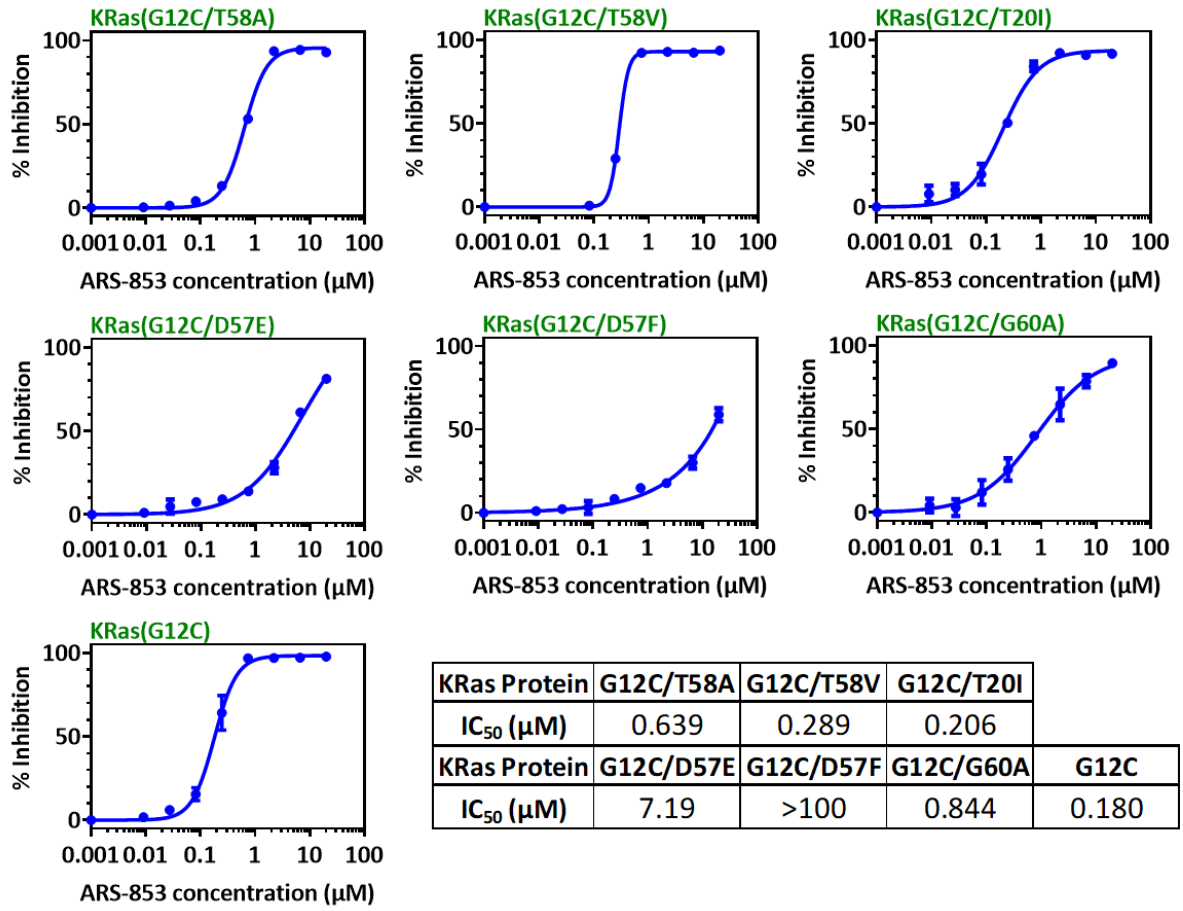

KRas Protein	G12C/T58A	G12C/T58V	G12C/T20I	
IC_{50} (μM)	0.639	0.289	0.206	
KRas Protein	**G12C/D57E**	**G12C/D57F**	**G12C/G60A**	**G12C**
IC_{50} (μM)	7.19	>100	0.844	0.180

Figure 9. The dose-response curves and IC_{50} values of ARS-853 in the SOS-driven KRas GDP/GTP exchange assay. The KRas(G12C/T58V) curve is missing points at two low concentrations. The Y-axis in each graph represents the inhibition of the exchange reaction.

3.5 Affinity of the KRas-mutant/Raf Interaction

To determine whether this study's double mutants retain interactions with downstream molecules such as Raf, we then developed a TR-FRET assay for measuring the KRas–Raf interaction. In this assay, we transformed KRas proteins from the inactive GDP form to the active GTP form with EDTA in the presence of an excess of GTP and then studied their binding to Raf. The results are shown in Figure 10. All 3 single mutants (G12C, G12V, and G12D) showed almost the same activity as that of KRas(WT). These results suggest that they can interact with the downstream molecule Raf as well as the wild-type protein can. Among all the G12C double mutants, KRas(G12C/T20I) showed the highest Raf binding activity (100% of the wild-type protein's activity). Although the KRas(G12C/T20I) mutant significantly reduces the GDP/GTP exchange rate, apparently, it has no impact on Raf binding. KRas(G12C/T58V), KRas(G12C/T58A), and KRas(G12C/G60A) also showed very good Raf binding (89%, 72%, and 70%, respectively, of the wild-type protein's activity). Although these three mutants showed very different GDP/GTP exchange rates, they had similar Raf binding activities. KRas(G12C/D57E) and KRas(G12C/D57F) showed only 17% and 2%, respectively, of the wild-type activity. The results suggest that mutations at Asp57 significantly change the protein conformation, thereby affecting GDP/GTP exchange rates and the interaction with Raf. As shown in Figure 6, D57E and D57F are not expected to be tolerated in the KRas(G12C)

binding cavity without conformational perturbations of the protein.

We noticed that the Raf binding activities, relative to that of KRas(WT), correlate with the ARS-853 IC_{50} values. For ARS-853 IC_{50} values less than 0.3 µM, as obtained for KRas(G12C), KRas(G12C/T20I), and KRas(G12C/T58V), the relative Raf binding activities are 89% or greater. For ARS-853 IC_{50} values of about 0.6 µM and 0.8 µM, as in the case of KRas(G12C/T58A) and KRas(G12C/G60A), the relative Raf binding activities are approximately 70%. The highest IC_{50} values are observed for KRas(G12C/D57E) (7.2 µM) and KRas(G12C/D57F) (>100 µM), which have marginal relative Raf binding activities (17% and 2%, respectively).

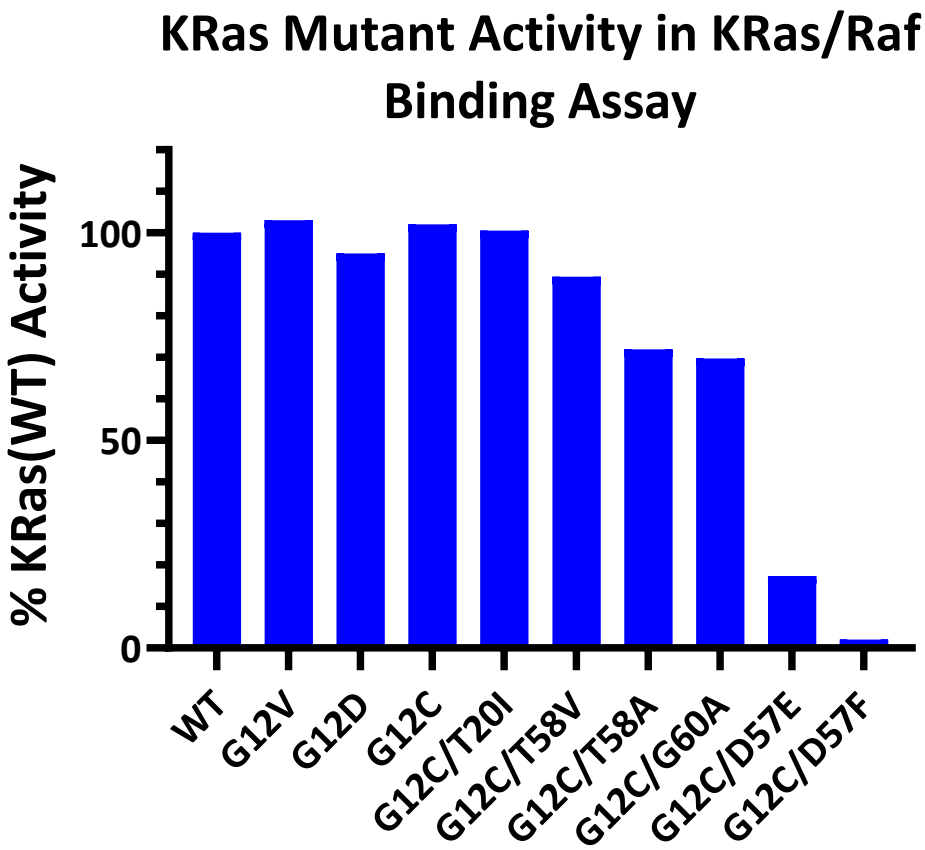

Figure 10. Relative Raf binding activities of KRas(WT) and various KRas single and double mutants.

4. Conclusions

KRas, for which there is extensive structural information, has been aggressively pursued as a drug target for decades, because it is the most frequently mutated protein involved in cancer. Despite the flurry of recent structural advances, KRas has presented serious drawbacks; "Sites B and C," as defined herein, are shallow surface features, and the transiently open "Site A" (the S-IIP) has only been successfully probed with covalent ligands. We developed a new strategy, based on the analysis of KRas and HRas X-ray structures, to ultimately discover non-covalent, small-molecule inhibitors that would bind to the transiently open switch II pocket (S-IIP) of KRas. The new strategy involved the design of a series of "synthetic" or "artificial" KRas mutations that are

individually introduced into KRas with the G12C natural mutation to create double mutants that would enhance assay sensitivity; in this study, we examined the introduction of T20I, D57E, D57F, T58A, T58V, and G60A. The goal of using these mutants was to induce greater overall flexibility of the KRas structure to allow the switch II pocket (S-IIP) to open more frequently in the absence of a C12-covalently bound ligand. This approach may be extended to other (non-G12C) KRas mutants and any other proteins for which low assay sensitivity is due to transient, high-energy, open-form binding sites.

We have developed various biochemical assays to study the activation of KRas and its interaction with the downstream molecule Raf. Using these assays, we have compared G12C, G12V, and G12D mutant activities with that of the wild-type protein. The results show that mutations at the G12 position have no effect on binding to Raf. Therefore, our results suggest that the hyperactivation of Raf signaling by the Ras mutation at the G12C position is not due to a stronger interaction with Raf. For the G12C-based double mutants, we found that KRas(G12C/T58V) and KRas(G12C/T58A) have the highest GDP/GTP exchange rates. In fact, their rates are higher than that of KRas(G12C) or KRas(WT). KRas(G12C/T58V) and KRas(G12C/T58A) show Raf binding activity (89% and 72%, respectively) that is comparable to that of KRas(WT). KRas(G12C/T20I) has only 24% of the KRas(G12C) GDP/GTP exchange rate. Yet, it has 100% of the KRas(G12C)/Raf binding activity. KRas(G12C/G60A) also has a very slow GDP/GTP exchange rate (7% of KRas(G12C)) and has about 70% of the KRas(G12C)/Raf binding activity. KRas(G12C/D57E) has about 40% of the KRas(G12C) exchange rate; however, it has only 17% of KRas(G12C)/Raf binding activity. As expected, due to the adverse impact of the mutation on protein conformation, KRas(G12C/D57F) does not show any significant GDP/GTP exchange or Raf binding.

The results of the biochemical assays provide preliminary support that some of the studied mutants demonstrate increased protein flexibility relative to that of KRas(G12C). However, we would like to determine whether our designed KRas double mutants have enhanced affinity, relative to that of KRas(G12C), for non-covalent binders at the S-IIP, by increasing protein flexibility or destabilization, as demonstrated through increased sensitivity in any of our biochemical and biophysical screens. We attempted to test our hypothesis with a covalent S-IIP ligand, specifically ARS-853. With ARS-853, we did not confirm or invalidate our hypothesis, because (as we believe) the results are largely indicative of the formation of the covalent bond between ARS-853 and Cys12 in the binding of the covalent ligand to the S-IIP, rather than serving as a measure of affinity for the full ligand.

Future studies will have to help validate the new strategy described in this article by noting differences in (a) assay sensitivity when non-covalent S-IIP compounds (verified by NMR or X-ray crystallography) are screened against KRas(G12C) and the associated double mutants and (b) X-ray crystallographic structures of the apo forms of KRas(G12C) and the double-mutant proteins.

References

1. Ostrem JML, Shokat KM, Direct small-molecule inhibitors of KRAS: from structural insights to mechanism-based design. Nat Rev Drug Discov. 2016;15(11):771–785. doi:10.1038/nrd.2016.139.

2. Vetter IR, Wittinghofer A. The guanine nucleotide-binding switch in three dimensions. Science. 2001; 294(5545):1299–1304. doi:10.1126/science.1062023.

3. Zenonos K, Kyprianou K. RAS signaling pathways, mutations and their role in colorectal cancer. World J Gastrointest Oncol. 2013; 5(5):97–101. doi:10.4251/wjgo.v5.i5.97.

4. Rajalingam K, Schreck R, Rapp UR, Albert Š. Ras oncogenes and their downstream targets. Biochim Biophys Acta. 2007;1773(8):1177–1195. doi:10.1016/j.bbamcr.2007.01.012.

5. Raepple D, von Lintig F, Zemojtel T, et al. Determination of Ras-GTP and Ras-GDP in patients with acute myelogenous leukemia (AML), myeloproliferative syndrome (MPS), juvenile myelomonocytic leukemia (JMML), acute lymphocytic leukemia (ALL), and malignant lymphoma: assessment of mutational and indirect activation. Ann Hematol. 2009;88(4):319–324. doi:10.1007/s00277-008-0593-6.

6. Maurer T, Garrenton LS, Oh A, et al. Small-molecule ligands bind to a distinct pocket in Ras and inhibit SOS-mediated nucleotide exchange activity. Proc Natl Acad Sci USA. 2012;109(14):5299–5304. doi:10.1073/pnas.1116510109.

7. Ahmadian MR, Stege P, Scheffzek K, et al. Confirmation of the arginine-finger hypothesis for the GAP-stimulated GTP-hydrolysis reaction of Ras. Nat Struct Biol. 1997;4(9):686–689. doi:10.1038/nsb0997-686.

8. Burns MC, Sun Q, Daniels RN, et al. Approach for targeting Ras with small molecules that activate SOS-mediated nucleotide exchange. Proc Natl Acad Sci USA. 2014;111(9):3401–3406; doi:10.1073/pnas.1315798111.

9. Kolch W. Meaningful relationships: the regulation of the Ras/Raf/MEK/ERK pathway by protein interactions. Biochem J. 2000;351(2);289–305. doi:10.1042/bj3510289.

10. Glaysher S, Bolton LM, Johnson P, Torrance C, Cree IA. Activity of EGFR, mTOR and PI3K inhibitors in an isogenic breast cell line model. BMC Res Notes. 2014;7(397):1–7. doi:10.1186/1756-0500-7-397.

11. Cosmic, v88, https://cancer.sanger.ac.uk/cosmic; last accessed on October 28, 2019.

12. Hunter JC, Manandhar A, Carrasco MA, Gurbani D, Gondi S, Westover KD. Biochemical and Structural Analysis of Common Cancer-Associated KRAS Mutations. Mol Cancer Res. 2015;13(9):1325–1335. doi:10.1158/1541-7786.MCR-15-0203.

13. Scheffzek K, Ahmadian MR, Kabsch W, et al. The Ras-RasGAP complex: Structural basis for GTPase activation and its loss in oncogenic Ras mutants. Science. 1997;277(5324):333–338. doi:10.1126/science.277.5324.333.

14. Kotting C, Kallenbach A, Suveyzdis Y, Wittinghofer A, Gerwert K. The GAP arginine finger movement into the catalytic site of Ras increases the activation entropy. Proc Natl Acad Sci USA. 2008;105(17):6260–6265. doi:10.1073/pnas.0712095105.

15. Papke B, Der CJ. Drugging RAS: Know the enemy. Science. 2017;355(6330):1158–1163. doi:10.1126/science.aam7622.

16. Maurer T, Garrenton LS, Oh A, et al. Small-molecule ligands bind to a distinct pocket in Ras and inhibit SOS-mediated nucleotide exchange activity. Proc Natl Acad Sci USA. 2012;109(14):5299–5304. doi:10.1073/pnas.1116510109.

17. Shima F, Yoshikawa Y, Ye M, et al. In silico discovery of small-molecule Ras inhibitors that display antitumor activity by blocking the Ras–effector interaction. Proc Natl Acad Sci USA. 2013;110(20):8182–8187. doi:10.1073/pnas.1217730110.

18. Ostrem JM, Peters U, Sos ML, Wells JA, Shokat KM. K-Ras(G12C) inhibitors allosterically control GTP affinity and effector interactions. Nature. 2013;503(7477):548–551. doi:10.1038/nature12796.

19. Patricelli MP, Janes MR, Li L-S, et al. Selective inhibition of oncogenic KRAS output with small molecules targeting the inactive state. Cancer Discov. 2016;6(3):316–329. doi:10.1158/2159-8290.CD-15-1105.7

20. Janes MR, Zhang J, Li L-S, et al. Targeting KRAS mutant cancers with a covalent G12C-specific inhibitor. Cell. 2018;172(3):578–589.e17. doi:10.1016/j.cell.2018.01.006.

21. Uniprot, the Universal Protein Resource, https://www.uniprot.org/; last accessed on October 28, 2019.

22. GenScript, 860 Centennial Ave. Piscataway, NJ 08854, USA, https://www.genscript.com/; last accessed on October 28, 2019.

23. Agilent, 5301 Stevens Creek Blvd. Santa Clara, CA 95051, USA, https://www.agilent.com/; last accessed on October 28, 2019.

24. Thermo Fisher Scientific, https://www.thermofisher.com/us/en/home.html; last accessed on October 28, 2019.

25. MilliporeSigma, 3050 Spruce St. St. Louis, MO 63103, USA, https://www.sigmaaldrich.com/united-states.html; last accessed on October 28, 2019.

26. Qiagen, https://www.qiagen.com/us/; last accessed on October 28, 2019.

27. GE Healthcare Life Sciences, https://www.gelifesciences.com/en/us/about-us; last accessed on October 28, 2019.

28. Bio-Rad, 2000 Alfred Nobel Drive, Hercules, California 94547, USA, https://www.bio-rad.com/featured/en/bradford-assay.html; last accessed on October 28, 2019.

29. PerkinElmer, 68 Elm Street, Hopkinton, MA 01748, USA, http://www.perkinelmer.com/; last accessed on October 28, 2019.

30. GraphPad Software, 2365 Northside Drive, Suite 560, San Diego, CA 92108, USA, support@graphpad.com.

31. Columbia Biosciences, 4985 Winchester Boulevard, Frederick, MD 21703, USA, https://columbiabiosciences.com/; last accessed on October 28, 2019.

32. Schrödinger Release 2016-1; Maestro, version 10.5.014; Schrödinger, LLC: New York, NY, 2016.

33. Berman HM, Westbrook J, Feng Z, et al. The Protein Data Bank. Nucleic Acids Res. 2000;28(1):235–242; the URL of the RCSB PDB is www.rcsb.org. doi:10.1093/nar/28.1.235.

34. Huang R, Southall N, Wang Y, et al. The NCGC pharmaceutical collection: a comprehensive resource of clinically approved drugs enabling repurposing and chemical genomics. Sci Transl Med. 2011;3(80):80ps16. doi:10.1126/scitranslmed.3001862.

35. Sastry GM, Adzhigirey M, Day T, Annabhimoju R, Sherman W. Protein and

ligand preparation: parameters, protocols, and influence on virtual screening enrichments. J Comput Aided Mol Des. 2013;27(3):221–234. doi:10.1007/s10822-013-9644-8.

36. Ganguly AK, Wang Y-S, Pramanik BN, et al. Interaction of a novel GDP exchange inhibitor with the Ras protein. Biochemistry. 1998;37(45):15631–15637. doi:10.1021/bi9805691.

37. Shima F, Ijiri Y, Muraoka S, et al. Structural basis for conformational dynamics of GTP-bound Ras protein. J Biol Chem. 2010;285(29):22696–22705. doi:10.1074/jbc.M110.125161.

38. Cox AD, Fesik SW, Kimmelman AC, Luo J, Der CJ. Drugging the undruggable RAS: Mission Possible? Nat Rev Drug Discov. 2014;13(11):828–851. doi:10.1038/nrd4389.

39. Ford B, Skowronek K, Boykevisch S, Bar-Sagi D, Nassar N. Structure of the G60A Mutant of Ras: Implications for The Dominant Negative Effect. J Biol Chem. 2005;280(27):25697–25705. doi:10.1074/jbc.M502240200.

40. Lito P, Solomon M, Li L-S, Hansen R, Rosen N. Allele-specific inhibitors inactivate mutant KRAS G12C by a trapping mechanism. Science. 2016;351(6273):604–608. doi:10.1126/science.aad6204.

41. Hansen R, Peters U, Babbar A, et al. The reactivity-driven biochemical mechanism of covalent $KRAS^{G12C}$ inhibitors. Nat Struct Mol Biol. 2018;25(6):454–462. doi:10.1038/s41594-018-0061-5.

42. Statsyuk AV. Let K-Ras activate its own inhibitor. Nat Struct Mol Biol. 2018;25(6):435–437. doi:10.1038/s41594-018-0066-0.

